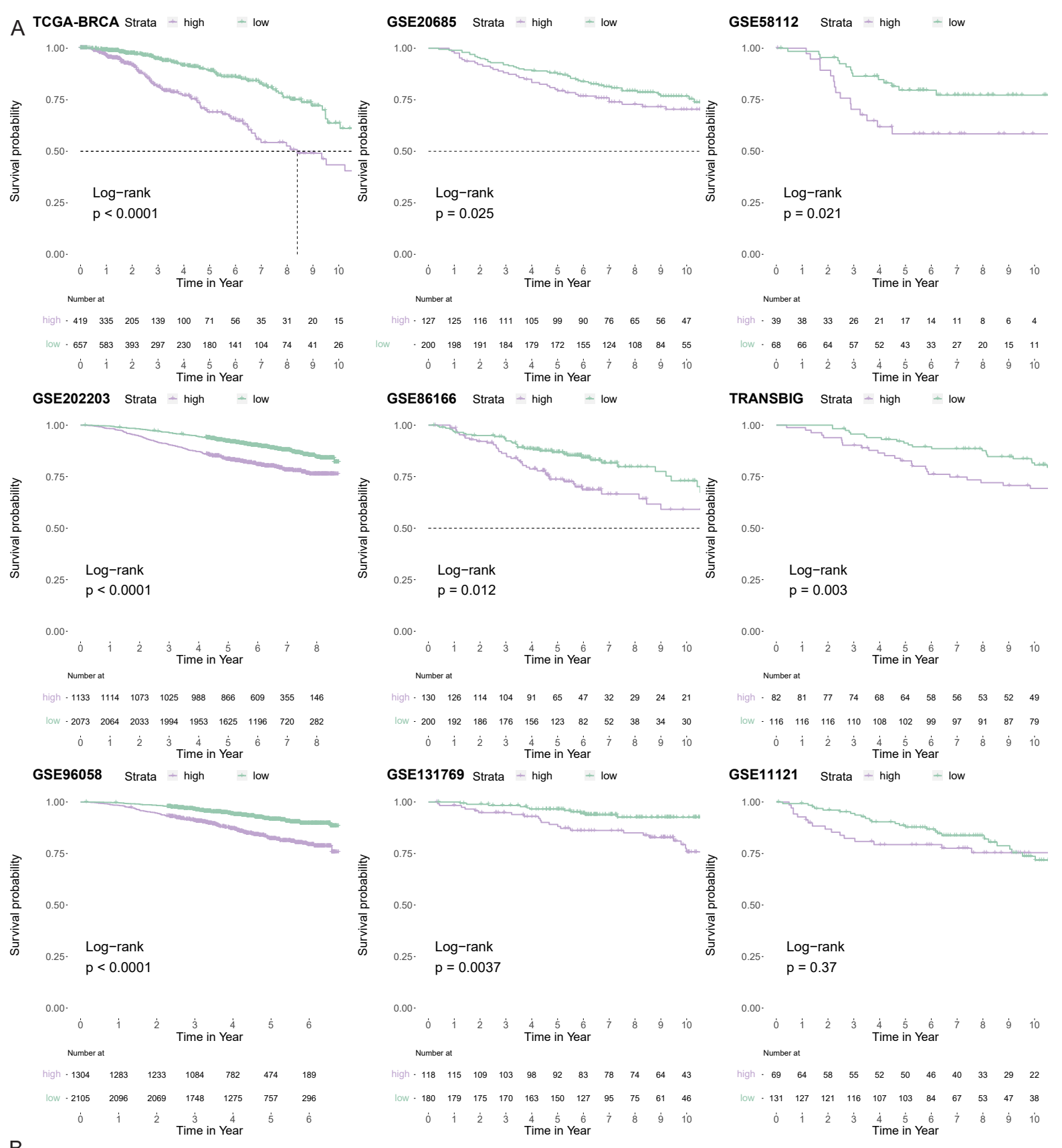

Figure S1. Evaluation of CMRS in 9 cohorts. (A) Kaplan-Meier curves of the CMRS in 9 cohorts. (B) Time-dependent ROC analysis for predicting OS at 1, 3, and 5 years.

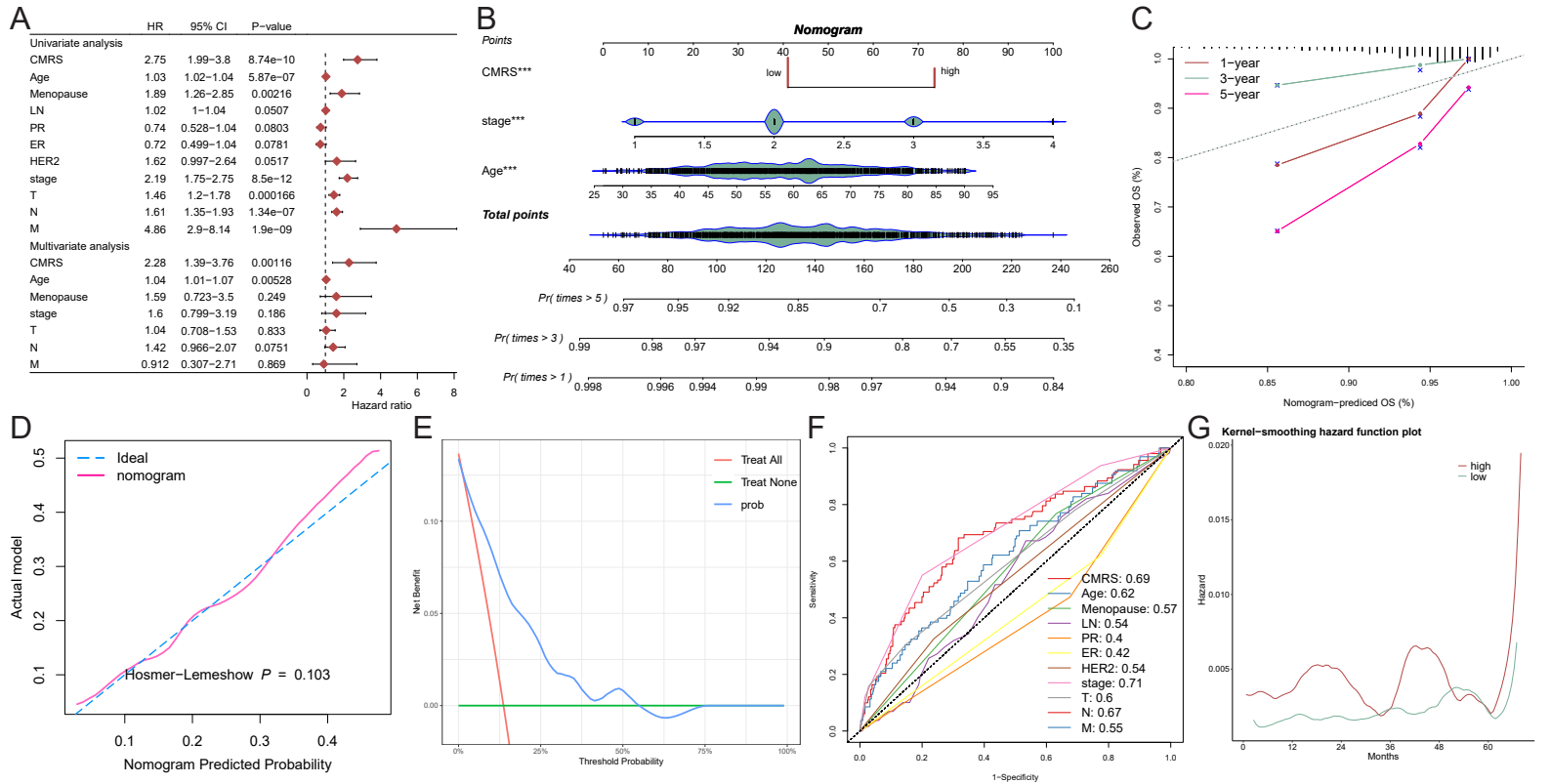

Figure S2. Prognostic characters of CMRS. (A) Forest plot illustrates the results of univariate and multivariate analyses, detailing hazard ratios (HR), 95% confidence intervals (CI), and p-values for various prognostic factors, providing a statistical view on the impact of these factors on patient outcomes. (B) A nomogram for predicting patient survival based on prognostic factors such as CMRS, stage, and age is shown; here, points are assigned to each factor, summed to a total, with corresponding survival probabilities indicated for different time frames (1, 3, and 5 years), offering a personalized survival prediction tool. (C) The calibration curve for the nomogram plots the nomogram-predicted survival probabilities on the x-axis against the observed survival rates at 1, 3, and 5 years on the y-axis, serving as a validation tool for the nomogram's accuracy. (D) Decision curve analysis (DCA) is displayed, showing the net benefit across a range of threshold probabilities for three different strategies: treating all patients, treating none, or using the CMRS score to guide treatment decisions, helping to evaluate the clinical usefulness of the CMRS score in making treatment decisions. (E) Receiver operating characteristic (ROC) curves for various factors used in the nomogram demonstrate the trade-off between sensitivity and specificity for predicting patient outcomes, aiding in assessing the predictive performance of the nomogram. (F) A kernel-smoothing hazard function plot estimates the recurrence rate for different CMRS subgroups, providing insights into the risk dynamics within these subgroups over time.

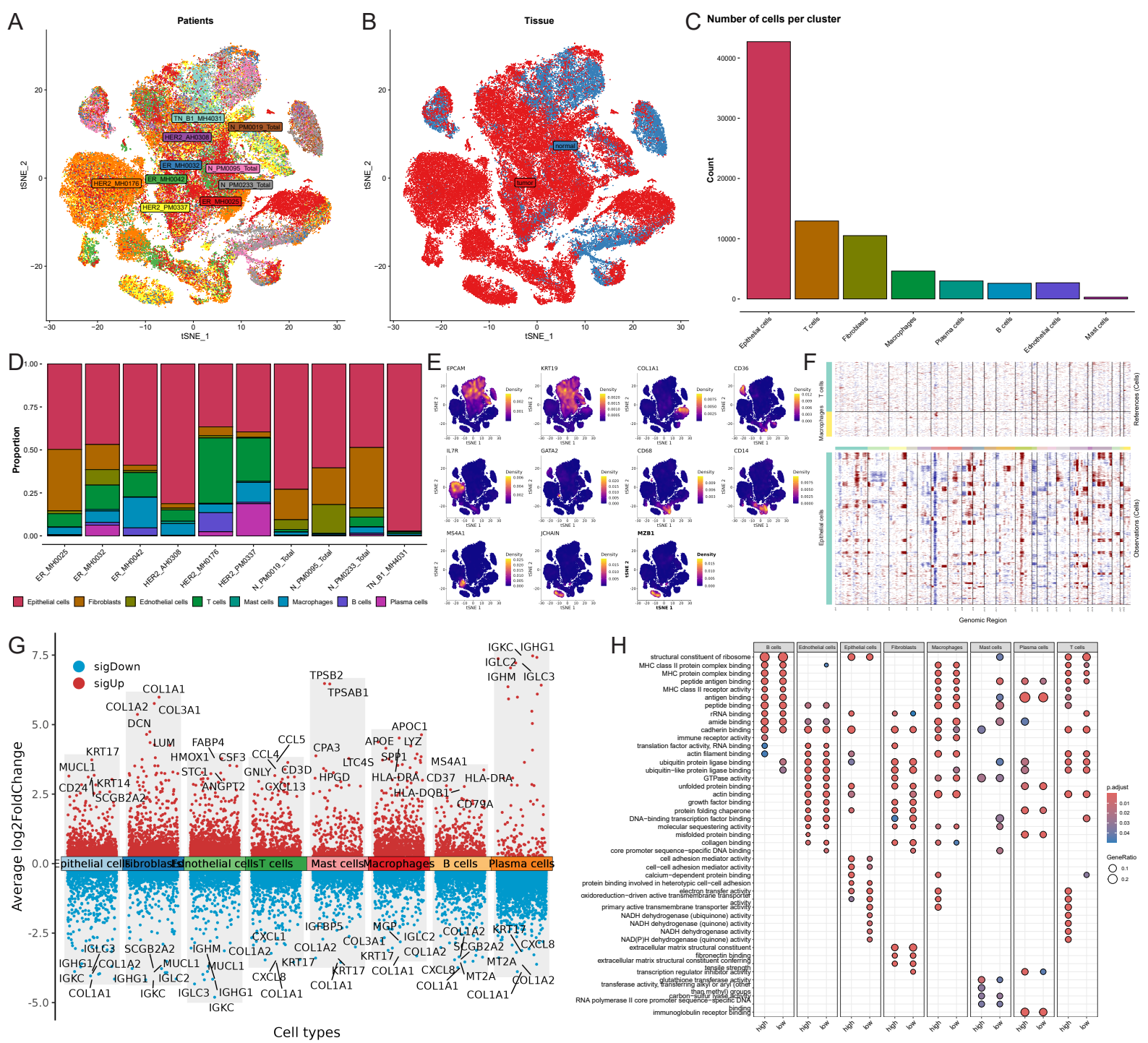

Figure S3. Comprehensive single-cell profiling of breast cancer. (A) A UMAP visualization illustrates the distribution of single cells from multiple breast cancer patients. (B) UMAP plot categorizes tissue type, with red dots representing tumor cells and blue dots indicating cells from normal tissue. (C) A bar graph displays the number of cells per cluster identified in the dataset, with the largest bar representing epithelial cells, indicating the prevalence of this cell type in the samples. (D) A stacked bar chart shows the proportion of different cell types found in individual patients, illustrating the variability in cellular composition between patients. (E) UMAP plots each highlight the density of specific marker genes across cells, providing insights into the expression patterns that may define cell function or status. (F) Inferring cancer cell using inferCNV. (G) A volcano plot illustrates differential gene expression across specific cell types, with genes that are significantly upregulated shown in red and downregulated in blue. Labels identify some of the most differentially expressed genes, offering clues to their potential roles in cancer biology. (H) A dot plot matrix reveals the probable involvement in specific biological processes of genes that are differentially expressed among each cell type, linking gene expression patterns to potential functional implications.

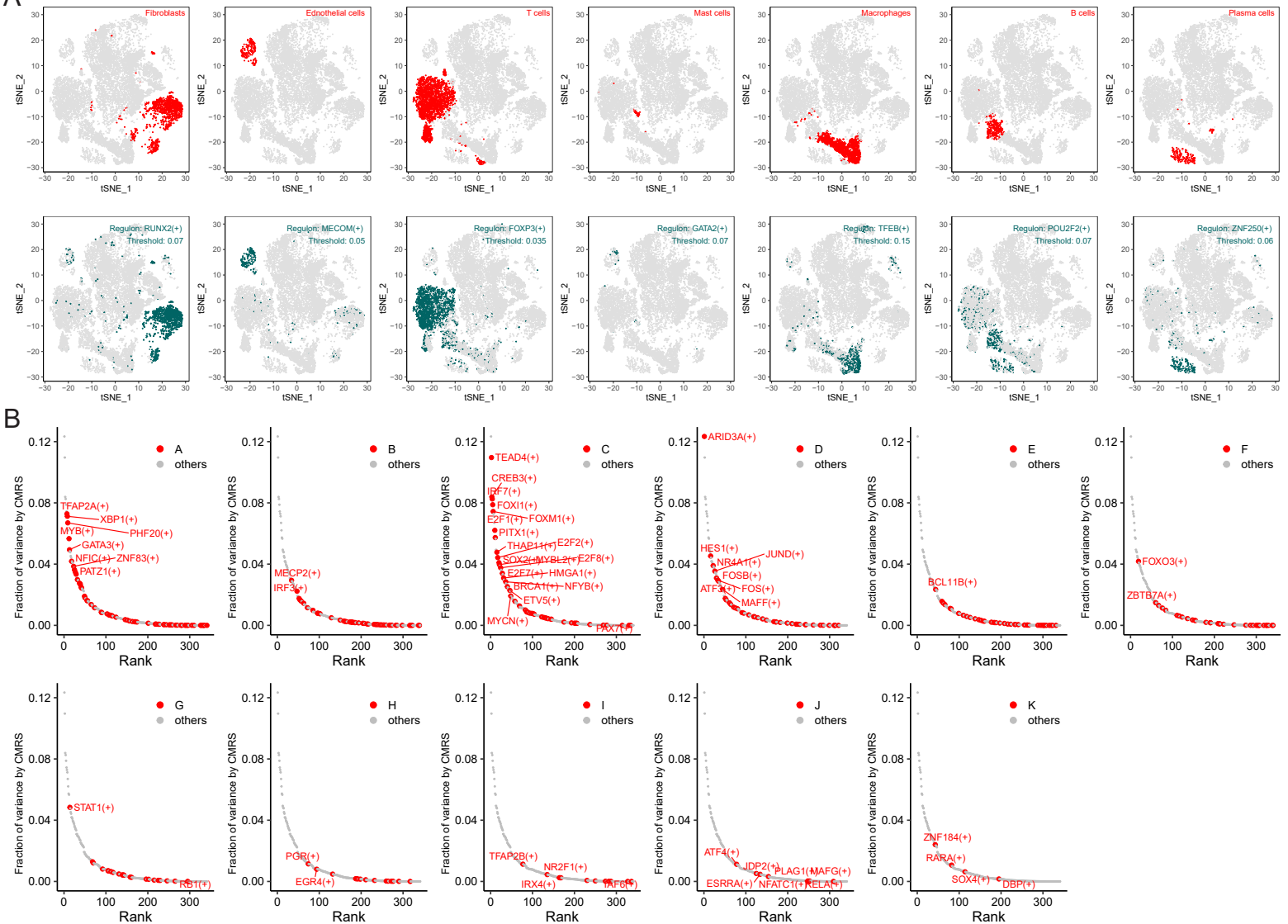

Figure S4. Transcription factor activity correlation and contribution analysis in cell types. (A) UMAP projections categorize samples by transcription factor activity, revealing distinct cell types based on their transcriptional profiles, aiding in the identification of unique cellular behaviors and properties. (B) Illustrates the contribution of different transcription factor groups to CMRS, with significant transcription factors highlighted and ranked based on their RSS, showcasing their regulatory impact on gene expression particularly in epithelial cells.